Urban Climate 17 (2016) 284–303

Contents lists available at ScienceDirect

Urban Climate

journal homepage: http://www.elsevier.com/locate/uclim

The effect of using a high-albedo material on the Universal Temperature Climate Index within a street canyon

P.J.C. Schrijvers [a,c,*], H.J.J. Jonker [a,c], S.R. de Roode [a,c], S. Kenjereš [b,c]

[a] Atmospheric Physics Section, Department of Geoscience & Remote Sensing, Faculty of Civil Engineering and Geotechnology, Delft University of Technology, Stevinweg 1, 2628CN Delft, The Netherlands
[b] Transport Phenomena Section, Department of Chemical Engineering, Faculty of Applied Sciences, Delft University of Technology, Julianalaan 136, 2628BL, The Netherlands
[c] J.M. Burgers Centre for Fluid Dynamics, Julianalaan 136, 2628BL, The Netherlands

ARTICLE INFO

Article history:
Received 19 September 2015
Received in revised form 13 December 2015
Accepted 22 February 2016

Keywords:
High-albedo material
Urban heat island
Adaptation measures
Universal Temperature Climate Index
Numerical simulation

ABSTRACT

This study investigates the effect of different high-albedo adaptation strategies on air temperature, mean radiant temperature and the Universal Temperature Climate Index (UTCI) for an idealized 2D street canyon. The used numerical model computes the heat transport in the canyon, and specifically takes into account the effect of multiple scattering of radiation. In general the mean radiant temperature has a much larger impact on the UTCI than the air temperature. Moreover, the mean radiant temperature exhibits strong spatial variations in the canyon due to its sensitivity to shading. The impact of albedo-differences on the UTCI is thus relatively small compared to the large shading effects. The best strategy to minimize the UTCI for the outdoor environment with building height to width ratio $H/W = 0.5$ is found to be a uniform albedo of 0.2. For $H/W = 1.0$, an albedo gradient from high at the bottom part to low at the top of the vertical walls showed the lowest UTCI. Although using high-albedo materials can mitigate the atmospheric urban heat island effect, it is very likely to increase pedestrian heat stress.

1. Introduction

Several studies (Whitman et al., 1997; Vandentorren et al., 2001; Baccini et al., 2008) have reported a relation between the ambient air temperature and the number of heat related deaths. This heat–mortality

* Corresponding author at: Atmospheric Physics Section, Department of Geoscience & Remote Sensing, Faculty of Civil Engineering and Geotechnology, Delft University of Technology, Stevinweg 1, 2628CN Delft, The Netherlands.
E-mail address: p.j.c.schrijvers@tudelft.nl (P.J.C. Schrijvers)

http://dx.doi.org/10.1016/j.uclim.2016.02.005
2212-0955/

relation, in combination with the Urban Heat Island effect (UHI, which is the phenomenon wherein the presence of buildings causes the temperature in the city to be higher than in its rural surroundings), poses a challenging problem on city planners to reduce the ambient air temperature inside the city. To achieve this air temperature reduction, the use of high-albedo materials for roofs or paving is often advocated, amongst others by Akbari et al. (2001) and Synnefa et al. (2008).

As a result, the use of these high-albedo materials is also incorporated as guidelines for architects and city planners. For instance, the New York High Performance Infrastructure Guidelines (2005) and Philadelphia High Performance Building Renovation Guidelines (2004) both recommend to use high-albedo pavement as a substitution for black asphalt to counter the local urban heat buildup. The general idea is that high-albedo materials absorb less solar radiation and thereby reduce the outdoor air temperature, which has been shown by many (Silva et al., 2009; Santamouris et al., 2012; Erell et al., 2014). For instance, Taha et al. (1999) studied the impact of large scale albedo changes for ten regions in the USA. A high-resolution regional weather forecast model was used, where the response of buildings and streets on the surface energy balance was specifically taken into account. The regions were characterized and simulated in reference- and modified-surface conditions. The results suggested that large-scale increases in the albedo and vegetative fraction can result in spatially-averaged decreases in mid-day air temperature of -0.5 K to -1.5 K during a typical summer day. The highest reduction found locally was -5 K.

Changing the albedo also influences the indoor air temperature (or the cooling load of obstacles, which is more often studied (Taha et al., 1988; Simpson and McPherson, 1997; Bretz et al., 1998). The effect of a different exterior albedo on the indoor air temperature has been demonstrated by Cheng et al. (2005), who performed idealized scale-experiments on a resolution of 1.5 m. These experiments were performed with separate black and white test-boxes and little insulation (20 mm thick waterproof plywood and 25 mm thick Styrofoam as interior thermal insulation). Both in summer and fall, the maximum indoor air temperature inside the black test box was roughly 12 K higher compared to the white test box.

Although a reduction in outdoor and indoor air temperature is considered positive, there are also downsides of using high-albedo materials. One of the adverse effects was demonstrated by Erell et al. (2014), in which the response of high-albedo materials on the outdoor pedestrian heat stress was investigated for four cities by using the Canyon Air Temperature model (CAT, Erell and Williamson (2006)). The CAT model uses meteorological measurement data from nearby rural locations to compute the canyon air temperature, wind speed and radiative properties inside the urban canyon. Radiative properties are based on the sky view factor and H/W ratio of the canyon, while urban wind speed and air temperature are computed from empirical formulations. The CAT model was used to compute the effect of different albedo values on the local urban climate inside the street canyon. The output of this model was then used to compute the Index of Thermal Strain (ITS model, Pearlmutter et al. (2007)), which is a pedestrian heat stress parameter. The ITS model empirically relates the clothing insulation, humidity of air, wind speed and the thermal and solar radiative fluxes to the thermal comfort of a standing human in units of Watt. For example, Erell et al. (2014) found that although a high-albedo material can lead to lower air temperatures, it may also cause a higher value of the heat stress, which is due to the increase in reflected radiation that can reach the pedestrian. The thermal stress is decreasing with increasing H/W ratio, independent of the albedo that is used. To quote the authors: “The results of this study indicate that local benefits, in terms of pedestrian thermal comfort, are likely to be marginal at best and that high-albedo paving materials may actually increase thermal stress in warm environments.” (Erell et al., 2014).

1.1. Goals

The current research aims to take the study by Erell et al. (2014) one step further. Instead of assuming a uniform albedo for the entire canyon as Erell et al. (2014), a variety of adaptation measures are tested. A building resolving model, called URBSIM (Schrijvers et al., 2015), is used which computes radiative transfer, heat conduction into the urban material, and ventilation within the urban canyon at a 1 m spatial resolution. Temperature and wind in the canyon are computed at this resolution (compared to a single point in the study by Erell et al., 2014). The different adaptation measures include differentiation between the north-facing and south-facing walls and albedo gradients along the vertical walls. In this way the impact of using different albedo values on the air temperature, mean radiant temperature and the Universal Temperature Climate Index (UTCI, Fiala et al., 2012) can be studied.

2. Methodology and used data

2.1. The numerical model

The effect of different albedo adaptation measures is tested by using the building resolving simulation model URBSIM that was developed and used in Schrijvers et al. (2015). The strength of URBSIM is that it hardly parametrizes the processes, but attempts to remain as close as possible to the physics. Radiation is solved by a Monte-Carlo model, which does not rely on view factor algebra, heat transport into the urban material is solved by the 1D heat conduction equation and a transient Reynolds-Averaged Navier–Stokes (RANS) Computational Fluid Dynamics (CFD) model is used for convective transport of heat, while the CFD model also takes into account buoyancy (Schrijvers et al., 2015; Kenjeres and Hanjalic, 1999, 2006, 2009; Kenjeres and ter Kuile, 2013; Kenjeres et al., 2015). At present, URBSIM is the only model available in literature, that combines Monte-Carlo radiation modelling and CFD at the street canyon resolving resolution. Only a short description is given here, and the reader is referred to Schrijvers et al. (2015) for model details and validation cases.

The Monte-Carlo radiation model computes individual photon-paths, which allows the assessment of the absorbed shortwave and longwave radiation at the surface, the longwave trapping effect and mean radiant temperature. The mean radiant temperature is defined as the temperature that a human body would have if all absorbed radiation is emitted again through longwave radiation (which assumes that the human body is in radiative equilibrium), and is computed by

$$T_{\mathrm{mrt}} = \sqrt[4]{\frac{S_{\mathrm{str}}}{\varepsilon_{\mathrm{p}}\sigma}} \tag{1}$$

where S_{str} is the local mean radiant flux density, ε_{p} the emissivity of the human body (with a standard value of 0.97) and σ the Stefan–Boltzmann constant. The mean radiant flux density is the amount of both shortwave and longwave radiation that is absorbed by a standing human body and is computed following Thorsson et al. (2007) as

$$S_{\mathrm{str}} = \left(1-\alpha_{\mathrm{p}}\right)\sum_{i=1}^{6} SW_i F_i + \varepsilon_{\mathrm{p}}\sum_{i=1}^{6} LW_i F_i \tag{2}$$

where α_{p} is the albedo of the human body (with a standard value of 0.3), SW_i the total shortwave radiative irradiance, LW_i the total longwave radiative irradiance and F_i a geometric factor representing a standing human body. The index i is used for the six directions where radiation is entering from. The geometric factor F has a value of 0.22 for radiation entering from each of the four cardinal points and 0.06 for radiation entering from the upward and downward directions (Thorsson et al., 2007). Since the current study is 2D, radiation entering from two cardinal points is missing (the faces occupying the 'air-sides' of the canyon), and is taken equal to that of the averaged radiation entering from the two known directions. This assumption can be regarded as computing the mean radiant temperature for a square, surrounded by obstacles.

The time dependent 1D heat conduction equation is used to compute the energy transfer from a building or ground surface into the underlying urban material (conductive heat flux). A zero-flux boundary condition is used for the temperature inside the urban material.

Wind speed, air temperature and the sensible heat flux are computed on a non-uniform grid, refined in the proximity of building walls and the ground, by a CFD model, which solves the unsteady RANS-equations for mass, momentum and temperature, as well as turbulent kinetic energy and dissipation through the standard k–ε model including the Durbin time scale (Durbin, 1996).

The three different model components, i.e. convective and radiative transport of heat in the canyon, and heat conduction through the ground and the walls, each compute a part of the surface energy balance, and are coupled through the surface temperature. A time step of 6 min is used, after which all fluxes are updated and a new surface temperature is computed. The main advantage of the presented model is that it computes in detail the interaction of the different processes at a building-resolving scale.

The input-parameters of the model are shown in Table 1. The location considered is that of Amsterdam (The Netherlands) in the middle of June, the month where the sun reaches the highest elevation angle in the Netherlands. Free stream air temperature is 293.15 K and is constant with height and time. The same

Table 1
Input constants for radiation, heat conduction into the urban material and the CFD model, where λ is the thermal conductivity of brick, ρ the density of brick, C_v the thermal heat capacity of brick, T_a the constant inlet air temperature and U the constant inlet wind speed.

	Radiation
Latitude	52° 22′ N
Longitude	4° 53′ E
Start day	2012-06-10 00:00
End day	2012-06-20 23:59
max SW_{dir}	833.1 W m^{-2}
max SW_{dif}	84.2 W m^{-2}
LW_{sky}	325.0 W m^{-2}
	Heat conduction
λ	0.72 W m^{-1} K^{-1}
ρ	1920 kg m^{-3}
C_v	835 J kg^{-1} K^{-1}
Δ wall	0.25 m
Δ ground	1.00 m
	CFD
T_a	293.15 K
U	4.0 m s^{-1}
Min cell width	1.0 m
Cell expansion	5%
Max cell size	25 m

holds for the free stream wind speed of 4 m s^{-1} (which is the average wind speed during the summer at Schiphol airport, nearby Amsterdam), such that only the solar radiation experiences a diurnal variation. These constant input parameters are used to reduce the complexity of the urban system. This idealized set-up does allow distinguishing between the different processes, and investigating the effect of the albedo change on the processes that govern the UTCI. For the same reason, both vegetation and vehicle traffic are omitted from this study. Although more advanced urban geometries have been studied (e.g. Tominaga et al. (2005) for 3D wind patterns, Brown and Delay (2001) for different building shapes and Theeuwes et al. (2014) for different heat transfer coefficients), these studies do not take into account the complex interplay between all processes at the building resolving scale.

The model uses an initial estimate of surface temperature, which is used to compute the air temperature and heat fluxes at the first time step after which all variables are able to freely evolve in time. Ten consecutive days are simulated. The simplified set-up with constant inlet conditions causes the results to become repetitive, in a statistical sense, after 5 days. We also note that the results do become independent of the prescribed initial conditions.

The model has been validated in Schrijvers et al. (2015). The Monte-Carlo radiation model was validated against effective albedo measurements conducted by Aida and Gotoh (1982), and showed a fair agreement between measurements and simulation, both for winter and summer conditions. In addition to experimental data, analytic results by Madronich (1987) were used to validate the computation of the radiative fluxes. The CFD model has been extensively validated by comparisons of velocity and concentration measurements (Kenjeres and ter Kuile, 2013; Kenjeres et al., 2015) from the Mock Urban Setting Test (MUST) wind tunnel experiments (Biltoft, 2002; Hilderman and Chong, 2004) and against wind tunnel measurements of wind speed and air temperature from Uehara et al. (2000). Both validation cases showed good agreement between the CFD model and experimental data. In addition to these validation cases, a grid convergence study has been conducted which indicated that grid convergence is reached by using a 1 m resolution (50×50 cells for $H/W = 1.0$ and 25×50 cells for $H/W = 0.5$).

In the current work, the model output is used to compute the UTCI. This is an apparent temperature, which takes into account air temperature, wind speed, radiation, humidity, metabolism of the human body and

clothing insulation worn by the subject. The UTCI is defined as the isothermal air temperature of the reference condition that would elicit the same dynamic response (strain) of the physiological model (Jendritzky et al., 2012). It has been developed as a standard measure for outdoor thermal conditions, and is designed to be applicable in all climates, seasons, and time and spatial scales. The advantage of using the UTCI is that all effects of an adaptation measure on the outdoor environment are captured in one number, that is directly related to the amount of heat stress.

From the UTCI-website (Broede, 2005), a Fortran90 sub-routine is available, which uses a sixth order polynomial function to compute the UTCI, which has been implemented in URBSIM. This function uses air temperature, mean radiant temperature, wind speed and relative humidity as input, and the energy balance between the human core and skin, between skin and clothing and the human metabolism is parametrized. The fit is valid for the following conditions:

- $223 \le T_a \le 323$ K
- $-30 \le (T_{mrt} - T_a) \le +70$ K
- $0.5 \le u_{10\ m} \le 17$ m s^{-1}

where T_a is the local air temperature and $u_{10\ m}$ the wind speed at 10 m height.
Since the local UTCI inside the canyon is investigated here, the wind speed at each grid cell centre inside the street canyon is used instead of the wind speed at 10 m height. In this way, changes in wind speed due to the different adaptation measures are taken into account.
Relative humidity is a very complex parameter to take into account into a micro-climate model, since it is dependent on evaporation, entrainment, boundary layer height and large scale advection. This would severely complicate the analysis, while it is not the main focus in the current investigation. Therefore, the relative humidity is taken as a constant, and an estimate is made of the maximum effect of relative humidity on the UTCI. By using different constant values of the RH (changing these in the postprocessing UTCI routine offline), an increase in the UTCI of 3.3 °C is found when changing the relative humidity from 0% to 100%.
The UTCI uses an assessment scale, which is displayed in Table 2. This assessment scale relates the UTCI temperature to the amount of heat stress that a human will experience. It must be noted that all temperatures throughout this manuscript are in units of Kelvin, except the UTCI, which is defined as the temperature in degrees Celsius to remain consistent with the literature on the subject.
A graphical representation of URBSIM is shown in Fig. 1. This flowchart displays the input parameters for URBSIM and the output parameters that are in turn used as input for the UTCI subroutine.

2.2. Adaptation measures

Different adaptation measures are tested for an idealized 2D geometry with square obstacles which are equal in height and spaced equally. The building width (B) is 25 m, distance between the obstacles (W) is 50 m, while building height is varied between $H = 25$ m ($H/W = 0.5$) and $H = 50$ m ($H/W = 1.0$). Ten obstacles are used in the domain to ensure a fully developed flow in the last canyon. The 2D geometry limits this study to cases where ventilation is mainly a 2D effect. For higher obstacles, it was found that the 2D geometry prohibits cross-flow through the canyon, which leads to a non-physical large stable stratification (Schrijvers et al., 2015). Therefore, these deep canyons are not considered here.

Table 2
Assessment scale of the Universal Temperature Climate Index (Bröde et al., 2012).

UTCI [°C]	Stress category
>+46	Extreme heat stress
+38 to +46	Very strong heat stress
+32 to +38	Strong heat stress
+26 to +32	Moderate heat stress
+9 to +26	No thermal stress

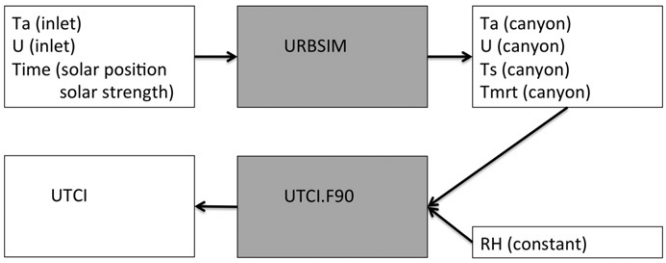

Fig. 1. Graphic representation of the different input and output of URBSIM to obtain the UTCI.

An east–west oriented canyon is used, such that building facades are either north-facing (shaded throughout the day) or south-facing (sunlit throughout the day). Since the current study is 2D, there is no solar azimuthal angle, and only the solar zenith angle is taken into account. Since the building facades are north-facing and south-facing, the 2D assumption is perfectly valid at solar noon.

As a first test, the albedo (α, which is referring to the reflectivity of solar radiation) of all canyon surfaces is varied between 0.2 (case 1), 0.4 (case 2) and 0.6 (case 3) respectively. These values for the albedo are also used for studying the impact of other adaptation strategies. An albedo of 0.2 corresponds to weathered asphalt, 0.4 to concrete and 0.6 to 'white-washed' surfaces. The outcome of varying longwave radiation is also quantified for different values of the emissivity ε, where ε is modified from 0.95 (case 2), 0.90 (case 4) and 0.85 (case 5) while the albedo is constant at $\alpha = 0.4$. Other test cases are shown in Fig. 2. Cases 6 and 7 investigate the effect of differentiating the albedo of the north-facing and south-facing walls, by using an albedo of 0.6 on one vertical surface and an albedo of 0.2 on the other surface. Cases 8 and 9 investigate walls with an albedo gradient, where a high top albedo (from a low-albedo bottom part to a high-albedo top part of the vertical wall) and a low top albedo (reversed) are used, respectively. Case 10 investigates a white roof ($\alpha = 0.6$ on all roof surfaces instead of the reference value of $\alpha = 0.4$). The hypothesis is that this reduces the ambient air temperature entering the canyon, which could cause a reduction of the UTCI. Case 11 investigates the impact of striping, where strips with different albedo values of 0.6 and 0.2 are used on the vertical walls. The reasoning is that this creates large spatial differences in surface temperature and therefore invigorates convection.

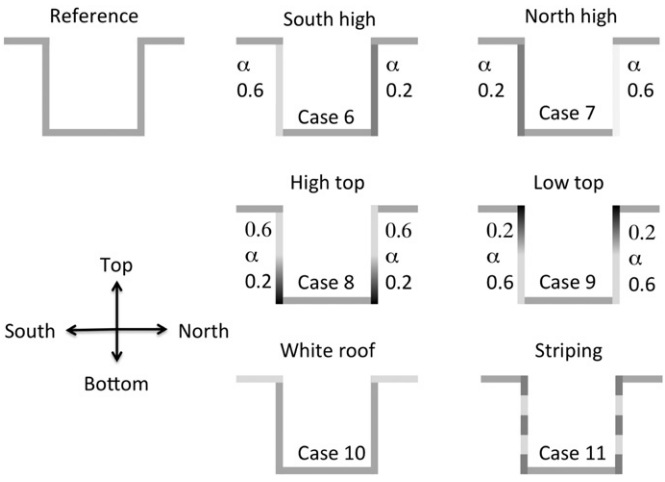

Fig. 2. Graphic representation of different albedo adaptation strategies. Cases with a uniform albedo ($\alpha = 0.2, 0.4, 0.6$) or uniform emissivity ($\varepsilon = 0.95, 0.90, 0.85$) are not shown here. Note that the solar position is always on the south side of the canyon.

3. Uniform canyon properties

This section will discuss the two cases in which the canyon is uniformly modified. Firstly, the albedo case is discussed, secondly the case with different uniform emissivity values.

3.1. Uniform albedo changes

3.1.1. Diurnal cycle

The first question addressed is how different albedo values affect the daily cycle of surface temperature inside the canyon. Therefore, time series of surface temperature are displayed in Fig. 3. Results for a single representative point centred on the road surface of the street canyon are shown for $H/W = 0.5$, and demonstrate a large variation in temperature, with the largest differences ranging from 290 K during the night to 319 K during day for the $\alpha = 0.2$ case. The case with $\alpha = 0.6$ displays differences between 290 and 306 K. The large influence of the albedo can be observed during the day when the point of interest is directly sunlit, with surface temperature differences of 7 K between the cases. However, the temperature differences during periods when the measurement point is in the shade (morning and afternoon) are small, indicating that the additional effect of multiple scattering is modest with changing the albedo. The impact of different albedo values is also limited during the night, where the surface temperature is mainly controlled by longwave radiation.

Since variations during the night are small, this study will only consider the results at solar noon of the last diurnal cycle.

3.1.2. Spatial distributions within a street canyon

Spatial changes as a result of different albedo values are shown in Fig. 4 for surface temperature (Fig. 4a), air temperature at 2 m height (Fig. 4b) and mean radiant temperature at 2 m (Fig. 4c). Solid lines are used for $H/W = 0.5$, while dashed lines are used for $H/W = 1.0$. Surface temperatures are plotted according to the inset in Fig. 4a, where all vertical surfaces are scaled to uniform height, to allow for direct comparison of different H/W ratios. Results for air temperature, mean radiant temperature and the UTCI are plotted along the width of the canyon (shown as canyon location), with 0 m at the north-facing wall and 50 m at the south-facing wall. Since both H/W ratios use a street width of 50 m, this does not require scaling. Canyon-average values at $z = 2$ m height for air temperature, mean radiant temperature and the UTCI are also summarized in Table 3 for all cases.

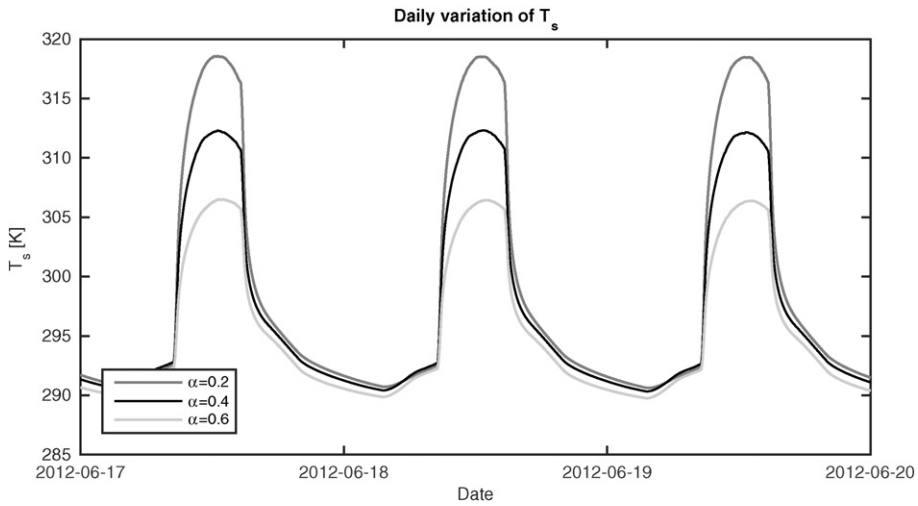

Fig. 3. Daily variation in surface temperature for one point in the centre of the street canyon ($H/W = 0.5$) for three different albedo values. The cases considered are with a uniform albedo.

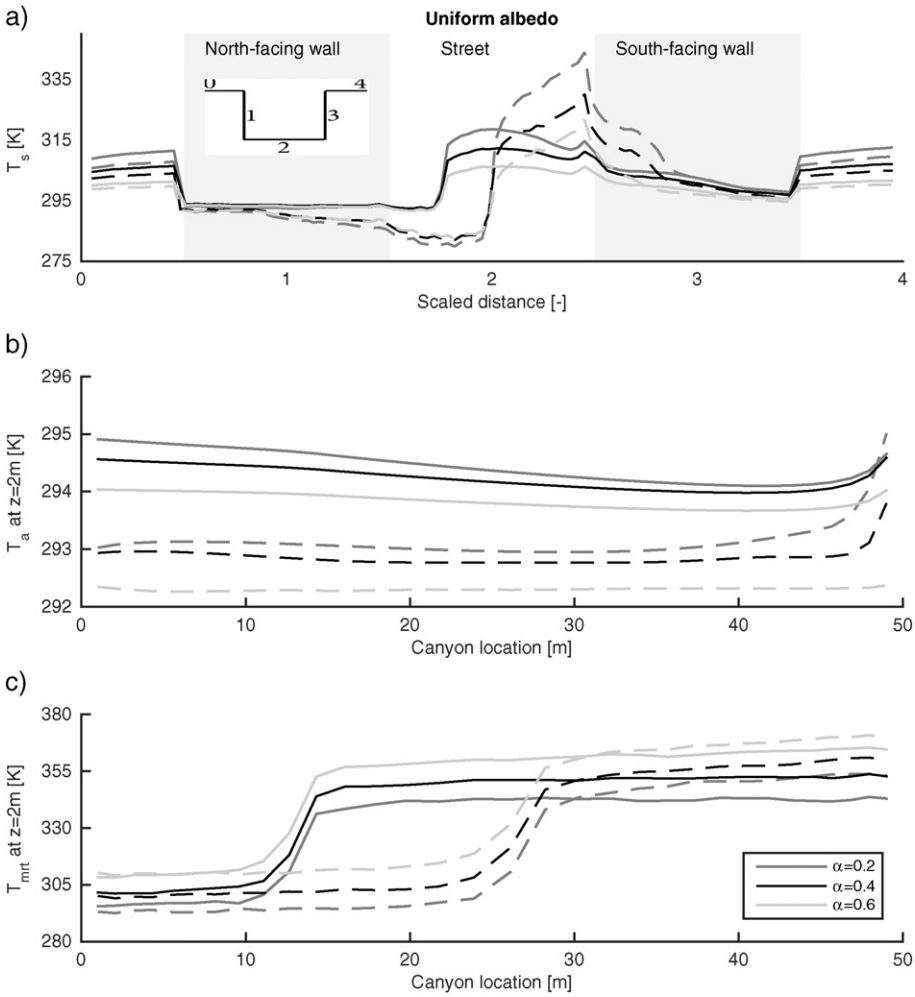

Fig. 4. Effect of albedo changes on surface temperature (a), air temperature at 2 m height (b) and mean radiant temperature at 2 m height (c). Grey scales are used for different cases, as indicated in the legend in the bottom panel. Solid lines are used for $H/W = 0.5$, while dashed lines are used for $H/W = 1.0$. Surface temperature is plotted according to the inset in the top panel. Air temperature and mean radiant temperature are shown as a function of the canyon location.

The results are shown for solar-noon, and reveal higher values of surface temperature near the street level for $H/W = 1.0$ in the sunlit region compared to $H/W = 0.5$, due to an increased number of multiple reflections (Fig. 4a). A low albedo increases surface temperature by as much as $+5$ K ($H/W = 0.5$) and $+14$ K ($H/W = 1.0$) at the sunlit part of the ground surface compared to the reference case, while the influence of changing the albedo is negligible in the shaded areas. Temperature is changed in the high-albedo case by -5 K ($H/W = 0.5$) and -8 K ($H/W = 1.0$) in the sunlit areas. For both H/W ratios, the impact of changing the albedo on surface temperature becomes smaller towards roof levels.

Air temperature is lower for the high-albedo case compared to the reference case (Fig. 4b). For $H/W = 0.5$, the difference in air temperature is (canyon averaged) $+0.2$ K for $\alpha = 0.2$ and -0.4 K for $\alpha = 0.6$ compared to the reference case ($\alpha = 0.4$). Note that the absolute air temperature is lower for $H/W = 1.0$ compared to $H/W = 0.5$ throughout the canyon. The difference in air temperature as a result of changing the albedo is comparable in magnitude to the findings of Erell et al. (2014), despite the large differences in case set-up,

Table 3
Effect of albedo and emissivity changes on air temperature, mean radiant temperature and the UTCI compared to reference case 2 with $\alpha = 0.4$ and $\varepsilon = 0.95$. Results are canyon averaged values at $z = 2$ m for $H/W = 0.5$ and $H/W = 1.0$ respectively. Case description is shown in Fig. 2.

Case name	Case description	ΔT_a [K]	ΔT_{mrt} [K]	ΔUTCI [°C]
Case 1	$\alpha = 0.2, \varepsilon = 0.95$	+0.2/+0.3	−8.1/−7.3	−1.9/−1.9
Case 2	$\alpha = 0.4, \varepsilon = 0.95$	0.0/0.0	0.0/0.0	0.0/0.0
Case 3	$\alpha = 0.6, \varepsilon = 0.95$	−0.4/−0.6	+9.5/+9.7	+2.0/+2.1
Case 4	$\alpha = 0.4, \varepsilon = 0.90$	0.0/+0.2	0.0/0.0	0.0/+0.3
Case 5	$\alpha = 0.4, \varepsilon = 0.85$	0.0/+0.5	0.0/−0.1	0.0/+0.4
Case 6	South low	+0.3/−0.7	−2.2/−2.7	−0.2/−1.1
Case 7	North low	−0.6/+0.2	+1.7/+0.2	−0.2/+0.3
Case 8	High top	−0.4/−0.1	−0.7/−1.2	−0.4/−0.4
Case 9	Low top	+0.8/0.0	−7.4/−8.6	−1.1/−2.7
Case 10	White roof	+0.1/−0.1	+0.4/+0.2	+0.2/+0.1
Case 11	Striping	+0.8/−0.6	−1.7/−0.7	+0.3/−0.3

inlet conditions and model that is used. This indicates that the impact of changing the albedo on air temperature is robust, i.e. similar for different conditions.

In addition to profiles at 2 m height, contours of air temperature are shown in Fig. 5 for $H/W = 0.5$ (left) and $H/W = 1.0$ (right) and the three different cases considered. The results indicate that a low albedo creates a warmer canyon, for which there is more absorbed radiation, surface temperature is higher and consequently air temperature is increasing. For $H/W = 0.5$, there is one recirculating vortex for all cases. For $H/W = 1.0$, there are two counter rotating vortices, where the warm south-facing wall creates buoyancy forces that are large enough to create a second vortex that spans the bottom part of the canyon. The air temperature profile at 2 m height reveals relatively modest changes compared to the remainder of the canyon. It must be realized that the conditions considered are idealized by using a fully developed flow in the canyon under consideration and that the model is 2D. Despite these simplifications, these results reveal an intricate interplay between a wind induced vortex and canyon buoyancy.

According to Eqs. (1) and (2), the mean radiant temperature (Fig. 4c) is not only influenced by the change in reflected shortwave radiation, but also by the emitted longwave radiation due to changing surface temperature. Mean radiant temperature displays the contrary effect to air temperature, where the high-albedo case shows a higher mean radiant temperature (+9.5 K for $H/W = 0.5$). The difference is however small when compared to the effect of shading, where T_{mrt} is over −40 K lower in the shaded areas compared to the sunlit areas. For $H/W = 1.0$, there is a larger area in the shade, with substantially lower canyon-averaged T_{mrt} as a consequence. In the sunlit part of the canyon, T_{mrt} is higher for $H/W = 1.0$ compared to $H/W = 0.5$ due to increased multiple reflections of shortwave radiation. Surprisingly, increasing building height has thus two different effects: there is a larger shaded area with lower heat stress, but due to the increase in multiple reflections the sunlit area experiences stronger heat stress.

T_{mrt} is controlled by the large contributions of direct shortwave radiation (which has a maximum value of 900 W m^{-2} in the sunlit area. The maximum value obtained is higher than the incoming 833 W m^{-2} from Table 1 due to multiple reflections) and the longwave trapping effect (with a maximum contribution of 700 W m^{-2}). This results in a T_{mrt} of 350 K (sunlit part, $H/W = 0.5, \alpha = 0.4$). When these values are compared to measurements of mean radiant temperature and radiative fluxes in the city of Göteborg, Sweden (Lindberg et al., 2008), the values obtained in the current study are higher than obtained from measurements, where a maximum T_{mrt} was found of 340 K for a large open square with $\alpha = 0.4$. The higher mean radiant temperature from the model is partly due to the 2D assumption, in which radiative fluxes from the east and west directions are taken equal to the average of the north and south directions. For the $\alpha = 0.4$ case, the horizontal fluxes originating from the direct short wave radiation in the sunlit area are 680 W m^{-2} and 320 W m^{-2} for the southward and northward directions, respectively. As a result, the current assumption uses its mean value 500 W m^{-2} for the east and westward flux, which results in a mean radiant temperature of 333.0 K. However, if the minimum value for the direct short wave radiation (in this case 320 W m^{-2}) would be used, the mean radiant temperature would reduce to 329.9 K. In addition to the 2D assumption, the current study considers highly idealized conditions, where there is no vegetation, no latent heat flux and clear skies, thereby allowing for these large radiative fluxes.

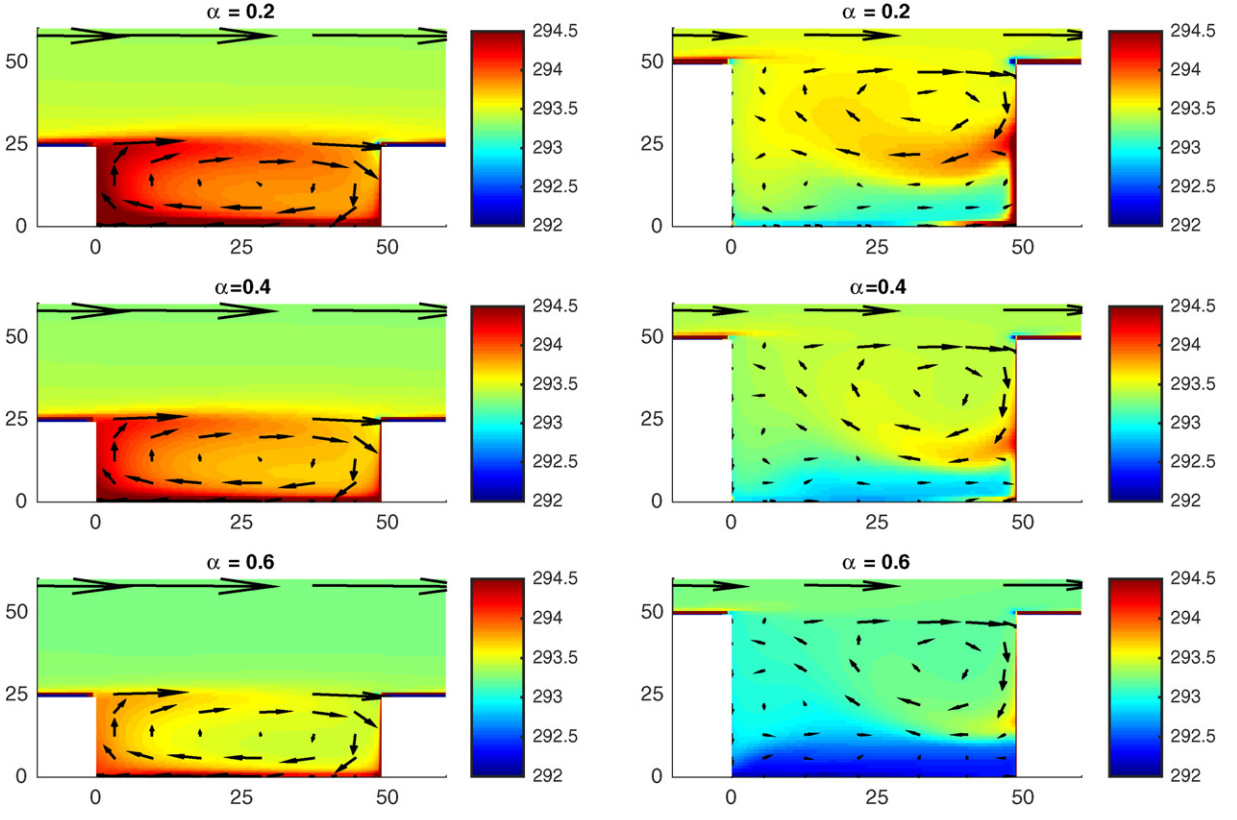

Fig. 5. Overview of air temperature for $H/W = 0.5$ (left panels) and $H/W = 1.0$ (right panels) when the albedo is changed uniformly over the entire canyon. The same colour axis is used for all sub-plots. Local wind is indicated by arrows, where the top arrows at $H/W = 0.5$ show a wind speed of 4 m s^{-1}.

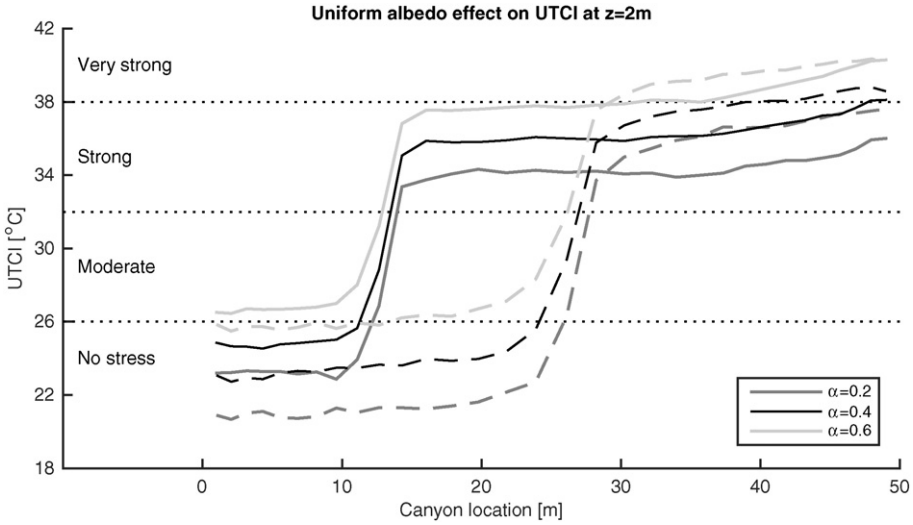

Fig. 6. The UTCI temperature for different values of the albedo, where the albedo is changed over the entire canyon. Solid lines indicate $H/W = 0.5$, dashed lines are used for $H/W = 1.0$.

The air temperature and the mean radiant temperature are both used as part of the input in the computation of the UTCI, which shows an increase for high-albedo canyons (see Fig. 6), by as much as $+2$ °C for both H/W ratios compared to the reference case. Using a low albedo changes the canyon-averaged UTCI by -1.9 °C for both H/W ratios. However, the influence of changing the albedo is small compared to the shading effect, which changes the UTCI in the shaded areas by as much as -12 °C, thereby indicating only 'moderate heat stress' if there is any stress at all. The large reduction of the UTCI in shaded areas is mainly due to the large decrease of direct shortwave radiation, which impacts the mean radiant temperature and therefore the UTCI. The local differences in air temperature cannot compensate the change in the mean radiant

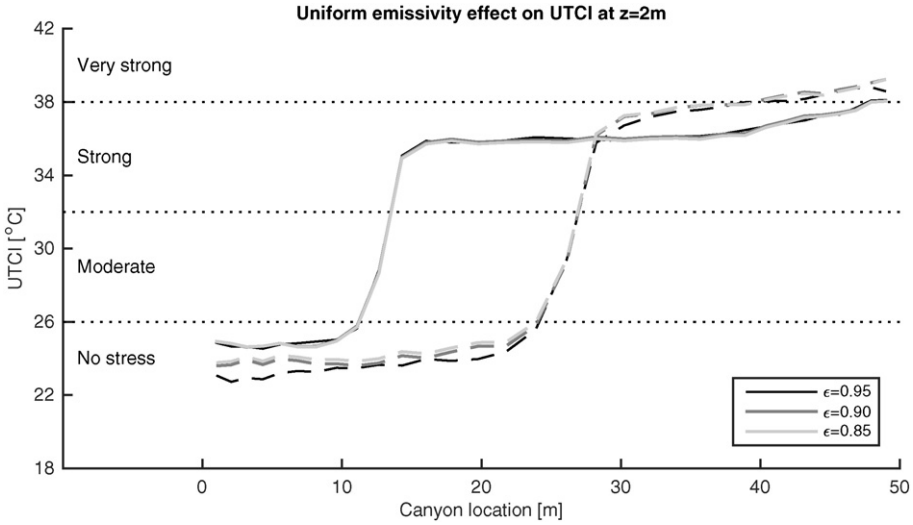

Fig. 7. Effect of different values of the emissivity on the UTCI, compared to the reference case with a uniform ε of 0.95. Solid lines are used for $H/W = 0.5$, dashed lines for $H/W = 1.0$.

temperature. For an increase in T_{mrt} of +15 K, air temperature should reduce by −7 K to maintain the same UTCI temperature for this case. Note that for this comparison, feedback effects from air temperature to the sensible heat flux, conductive heat flux, surface temperature and mean radiant temperature are neglected, which gives just a very coarse indication of the required temperature increase.

Erell et al. (2014) found that for any albedo value the thermal stress for a pedestrian in the middle of the street canyon is decreasing with increasing H/W ratio. A similar result is obtained in the current study for the shaded part of the canyon. By contrast, in the sunlit part, the thermal stress increases due to the effect of multiple reflections at this location.

3.2. Uniform emissivity effect

In addition to changing the canyon albedo, a varying emissivity is investigated. There are currently coatings available that can be applied on the glass surface, such that emissivity is reduced. Unfortunately,

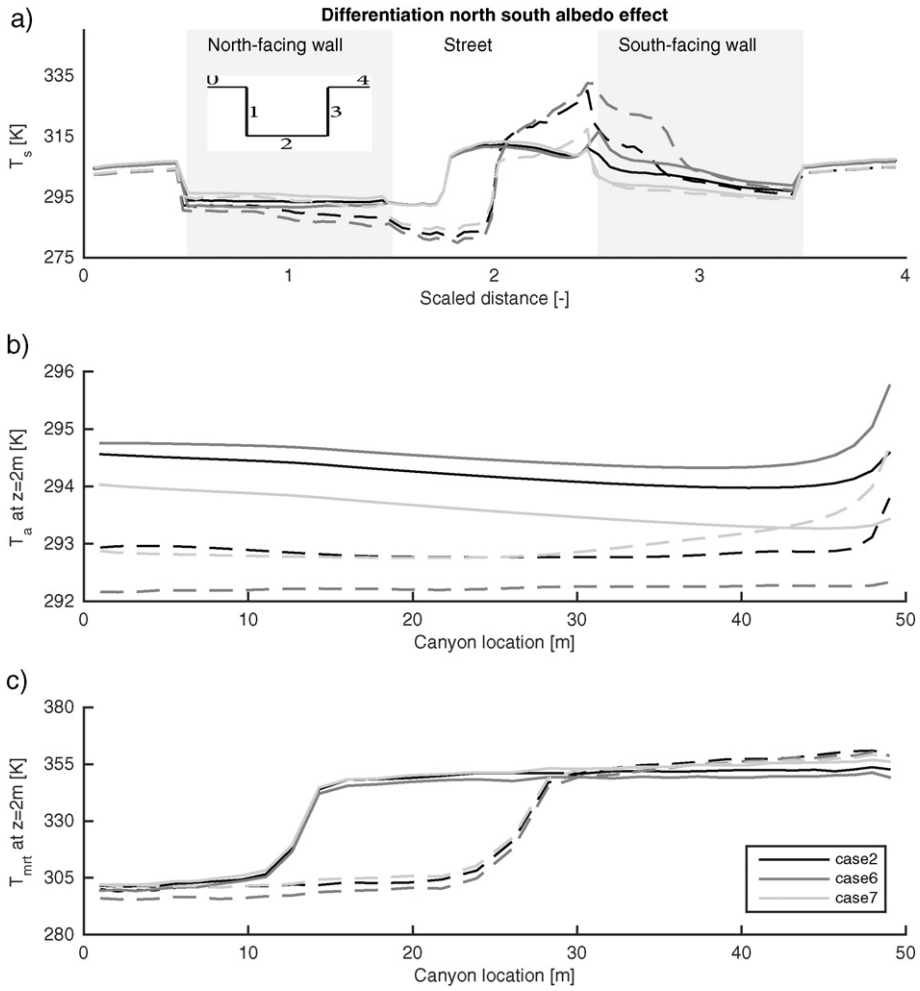

Fig. 8. Effect of using a high-albedo north-facing (case 6) and south-facing (case 7) wall on surface temperature (a), air temperature at 2 m height (b) and mean radiant temperature at 2 m height (c). A graphic representation of the cases is displayed in Fig. 2. Solid lines are used for $H/W = 0.5$, while dashed lines are used for $H/W = 1.0$. Surface temperature is plotted according to the inset in the top left panel. Air temperature and mean radiant temperature are shown as a function of the canyon location.

the combined effect of glass including this emissivity-reducing coating is usually not given. Therefore, this remains an academic case, to investigate the possible impact of low-emissivity materials. Noting that according to Kirchhof's law the spectral emissivity equals the absorptivity of infrared radiation, one could hypothesise that decreasing the emissivity could lead to a feedback effect on surface temperature (less absorbed radiation from the sky, lower surface temperature, less longwave trapping, lower surface temperature, etc.), which could significantly lower the UTCI. The second consequence of reducing the surface emissivity is an increase in the surface temperature, due to the reduced emission of longwave radiation from the surface. In the current study, the total impact of changing the emissivity is investigated, and the two separate mechanisms discussed above are not investigated separately.

The effect of varying the emissivity on the UTCI is visualized in Fig. 7 and in Table 3 for the different cases. A decrease in the emissivity from 0.95 to 0.85 did not affect the UTCI for $H/W = 0.5$ and increased the UTCI by $+0.4$ °C for $H/W = 1.0$.

Absorbed infrared radiation at the surface is decreasing with a lower emissivity. However, this decrease is much smaller compared to changing the albedo of solar radiation. Due to the high value of the emissivity, the amount of energy involved with multiple reflections is smaller. Since the change in surface temperature is small, there is also little ramification on the longwave trapping effect. The UTCI is therefore hardly changing. For $H/W = 1.0$, air temperature is increasing more than the mean radiant temperature is decreasing, leading to an increase in the UTCI.

4. Sensitivity studies

4.1. Differentiating albedo of the street canyon vertical walls

In this section, case 6 (a high-albedo on the north-facing wall) and case 7 (with a high-albedo for the south-facing wall) are compared to the reference case 2 with a uniform albedo (see Fig. 2 for a graphic representation). Note that the average albedo over all surfaces remains equal for these cases.

Varying the albedo of the vertical walls reduces the surface temperature for case 7 (Fig. 8a) at the lower corner between the south-facing wall and ground by -8 K (-12 K) for $H/W = 0.5$ ($H/W = 1.0$). The north-facing wall is heated by $+2$ K compared to the reference case for both H/W ratios. The heating of the north-facing wall can be explained from the fact that the surface does not only absorb more solar radiation due to the lower albedo, but also due to the increased amount of received radiation that is reflected by the

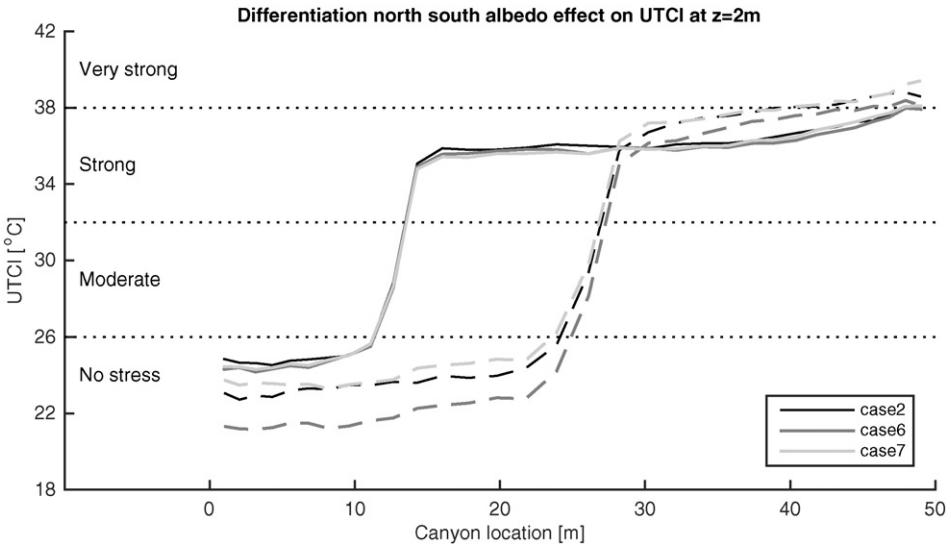

Fig. 9. Effect of differentiating the albedo of north-facing and south-facing walls on the UTCI, compared to the reference case with a uniform ε of 0.95. Solid lines are used for $H/W = 0.5$, dashed lines for $H/W = 1.0$.

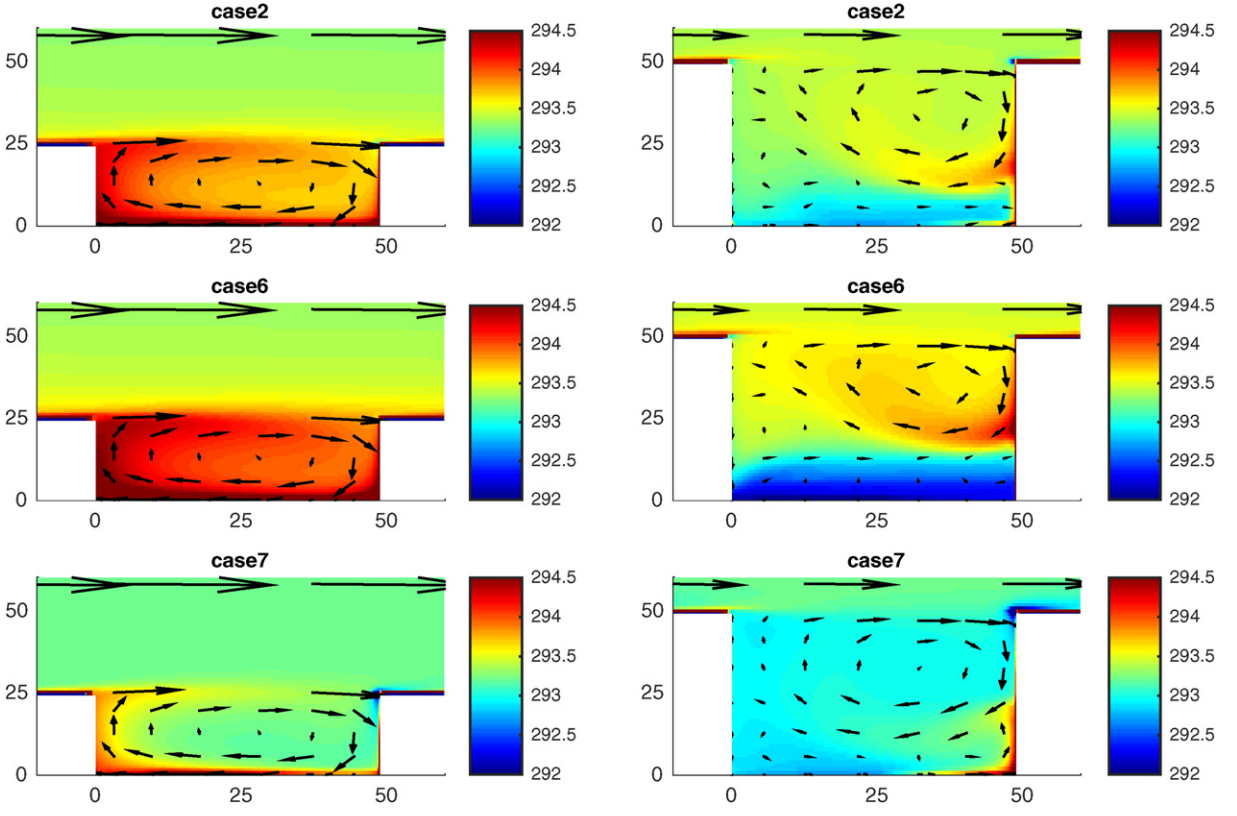

Fig. 10. Overview of air temperature for $H/W = 0.5$ (left panels) and $H/W = 1.0$ (right panels) for the reference case (uniform albedo of 0.4, top panels), case 6 (high-albedo north-facing wall, middle panels) and case 7 (high-albedo south-facing wall, bottom panels). The colour scale used is identical to the colour-scale used in Fig. 5.

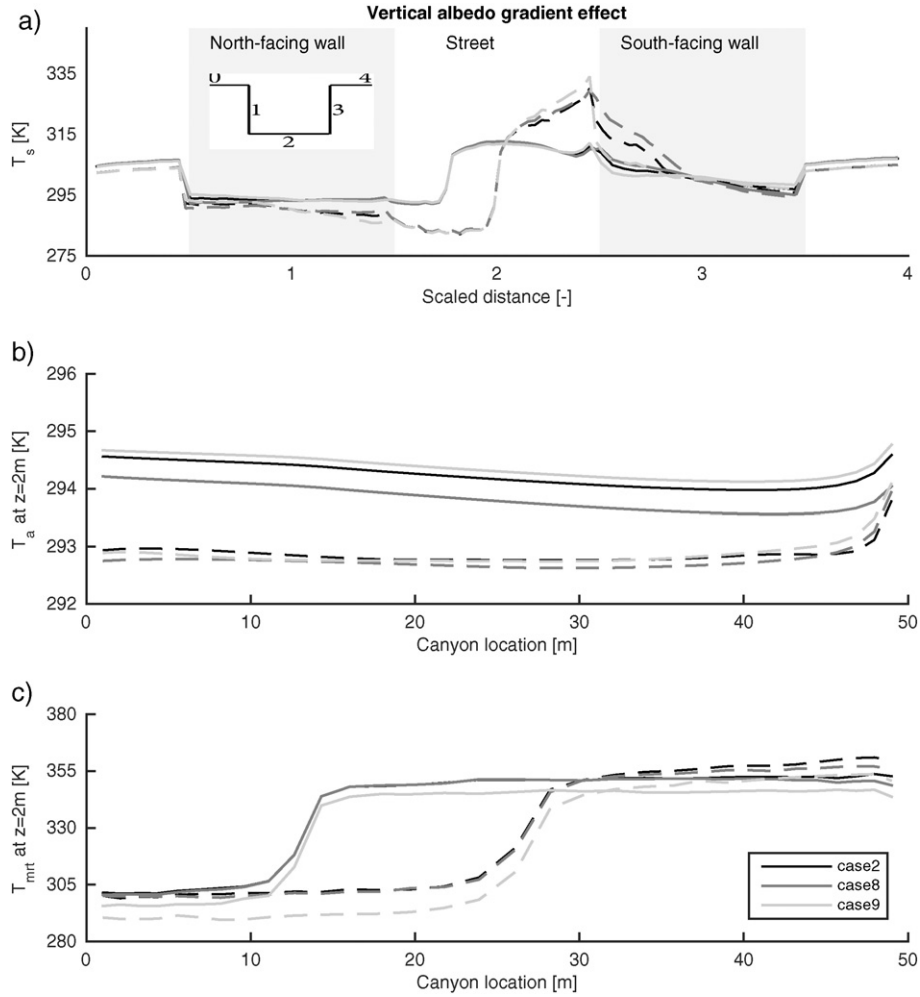

Fig. 11. Effect of vertical albedo gradients on surface temperature (a), air temperature at 2 m height (b) and mean radiant temperature at 2 m height (c). Case 8 uses a high albedo at the top part of the vertical wall, case 9 a low albedo.

south-facing wall. The impact of a high albedo for the north-facing wall (case 6) is however smaller, with only a reduction in surface temperature of −1.5 K (−3.0 K) for $H/W = 0.5$ ($H/W = 1.0$) at the north-facing wall, while the surface temperature of the low-albedo south wall is increasing by +7 K (+15 K) for $H/W = 0.5$ ($H/W = 1.0$).

Air temperature profiles (Fig. 8b) reveal differences of up to +0.7 K for case 7. The results are also summarized in Table 3. However, the most interesting phenomena can only be seen from the spatial air temperature patterns, as shown in Fig. 10. For $H/W = 0.5$, the canyon for case 7 is found to be colder than the reference case, particularly due to the lower surface temperature at the south-facing wall. For $H/W = 1.0$, case 7 results in a higher air temperature at the bottom of the canyon, which is due to a change in vortex dynamics between the different cases. The reference case and case 6 exhibit two counter rotating vortices, where cold air is trapped at the lower part of the canyon. For case 7, the surface temperature at the south-facing wall is lower, there is less warm air rising and the forced convection (due to the free stream air flow) is larger than natural convection (due to buoyancy forces). This results in one single vortex which spans the whole canyon. The considered adaptation measures demonstrate different effects on air temperature for different H/W ratios. This justifies including CFD modelling, as it illustrates how a change in the albedo can completely

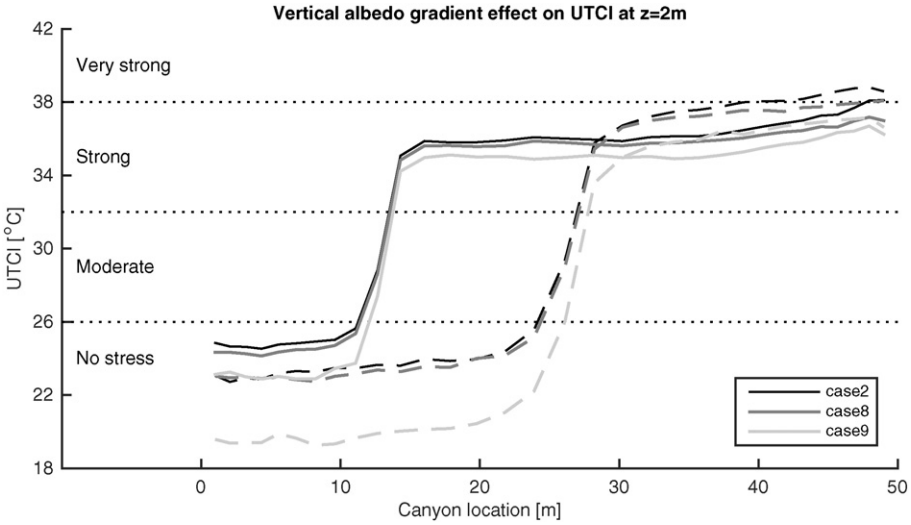

Fig. 12. Effect of vertical albedo gradients on the UTCI, compared to the reference case with a uniform albedo of 0.4. Case 8 uses a high albedo at the top part of the vertical wall, case 9 a low albedo. Solid lines are used for $H/W = 0.5$, dashed lines for $H/W = 1.0$.

alter the air flow patterns. It is recommended to investigate these phenomena with more advanced models (for instance the algebraic flux model) further, since it is known that k–ε turbulence models can have difficulties with complex buoyant flows.

The mean radiant temperature is shown in Fig. 8c, and displays a decrease for case 6 of -2.5 K while it is increased by $+1.7$ K ($H/W = 0.5$) and $+0.2$ K ($H/W = 1.0$) for case 7.

Despite the changes in surface temperature, air temperature and mean radiant temperature, the effect of differentiating the albedo of the north-facing and south-facing walls on the UTCI is small for $H/W = 0.5$ (see Fig. 9). Both cases with a different albedo at either side of the buildings reduce the UTCI by -0.2 °C.

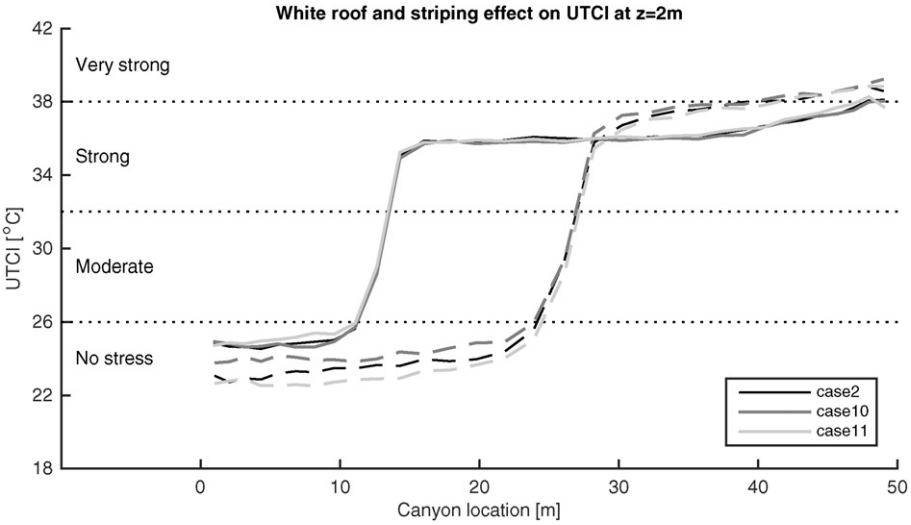

Fig. 13. Effect of white roof (case 10) and striping (case 11) on the UTCI, compared to a uniform albedo of 0.4 (case 2). Solid lines are used for $H/W = 0.5$, dashed lines for $H/W = 1.0$.

For $H/W = 1.0$, larger differences are present, where case 6 reduces the UTCI by −1.1 °C, while case 7 with the high-albedo south-facing wall increases the UTCI by +0.3 °C. Both H/W ratios indicate that a low-albedo south-facing wall reduces the UTCI, despite the increase in air temperature, again demonstrating the large impact of shortwave radiation.

4.2. Vertical albedo gradients

Instead of changing the albedo of the entire wall, two cases are considered where there is an albedo gradient on the vertical walls (case 8, which uses a high-albedo at the top, and case 9 which uses a low albedo at the top, see Fig. 2).

Differences in surface temperature due to the varied albedo values are mainly present at the bottom part of the south-facing wall (Fig. 11a), with maximum changes of +7 K for case 8 and −7 K for case 9.

Larger differences in air temperature are found (Fig. 11b) for the albedo gradient case compared to the uniform albedo cases, with a decrease in air temperature of −0.4 K ($H/W = 0.5$) for case 8 and an increase of +0.8 K for case 9 ($H/W = 0.5$). With a high albedo at the upper part of the canyon, there is less heating of ambient air at the top of the canyon, which has a lasting impact on the remainder of the canyon. The recirculating air is heated inside the canyon, but the canyon as a whole remains colder compared to the reference case.

For each of the vertical albedo cases, the mean radiant temperature is surprisingly decreasing as compared to the reference case (Fig. 11c). For case 9, the mean radiant temperature decreases by roughly −8 K, while this is −1 K for case 8. For a low albedo at the top part of the canyon, more shortwave radiation is absorbed at the top of the canyon, and less radiation is reflected towards the ground surface, and is present for both direct shortwave radiation and diffuse shortwave radiation. For case 8, the high-albedo top of the canyon reflects more radiation into the canyon, which is absorbed at the lower parts of the vertical walls.

If all effects are combined into the UTCI (Fig. 12), a decrease is shown for both cases. Case 8 exhibits a decrease of −0.4 °C for both H/W ratios, while case 9 decreases the UTCI by −1.1 °C for $H/W = 0.5$ and −2.7 °C for $H/W = 1.0$. The decrease in the UTCI for $H/W = 1.0$ is larger for case 9 than a uniform albedo of 0.2 and is thereby the most efficient measure to reduce the outdoor thermal comfort found in the current study.

4.3. White roof and striping

Results for the UTCI for cases 10 (white roof) and 11 (striping) are displayed in Fig. 13 and Table 3 and display small changes in the UTCI compared to the reference case. For case 10, there is a reduction in ambient air temperature as hypothesised in Section 2.2 for $H/W = 1.0$, but this is small (−0.1 K). The reduction in ambient air temperature is not present for $H/W = 0.5$. Remarkably, mean radiant temperature is increasing, which leads to an increase in the UTCI of +0.2 °C for $H/W = 0.5$.

Case 11 (striping of vertical surfaces) has a large impact on surface temperature, where local differences of up to 10 K are found compared to the reference case. However, such large temperature differences are not present when air temperature is considered, with an increase for $H/W = 0.5$ (+0.8 K) but a decrease for $H/W = 1.0$ (−0.6 K). Mean radiant temperature reveals opposite effects to air temperature, which results in a small impact on the UTCI for $H/W = 0.5$ (+0.3 °C) and a decrease in the UTCI for $H/W = 1.0$ of (−0.3 °C). It is unclear why striping demonstrates differences in the UTCI for the different H/W ratios.

5. Discussion

The present study is an extension of the work by Erell et al. (2014), who performed simulations with a uniform albedo for different H/W ratios in different cities. A more advanced model is used compared to Erell et al. (2014), which couples a CFD model, a Monte-Carlo radiation model and thermal diffusion through the 1D heat conduction equation, but finds similar results for the case with a uniform albedo. However, Erell et al. (2014) only considered a standing person in the middle of the canyon, while the entire canyon is investigated in the current study. As a second extension, different albedo adaptation strategies are used, which showed that using an albedo gradient (from a high-albedo at the top part of the vertical wall to a

low-albedo at the bottom part) can be more beneficial in terms of lowering the heat stress compared to a uniform low albedo for $H/W = 1.0$.

The maximum effect that is obtained by using different albedo adaptation strategies is about −2 °C on the UTCI, and is independent of H/W ratio. Surprisingly, increasing the building height reveals two distinct effects: there is a larger shaded area with a lower heat stress, but due to the increase in multiple reflections the sunlit area experiences stronger heat stress, especially near the sunlit south-facing wall. The UTCI is reduced by up to −12 °C in shaded areas compared to the sunlit areas, almost independent of the case that is investigated. The shadow-effect is also seen for the different H/W ratios: for every case investigated, the canyon averaged UTCI at 2 m is lower for $H/W = 1.0$ compared to $H/W = 0.5$, which is also what Erell et al. (2014) found. Therefore, it might be worthwhile to investigate artificial shading measures, which provide shading during the day but can be opened during night (increase ventilation and reduce longwave trapping).

The present study also demonstrated that changing the albedo values can alter the vortex dynamics inside a street canyon. Although idealized conditions are used here, buoyancy forces respond to the various measures, which encourages further investigations with more advanced CFD models. The effect of changing surface temperature on vortex dynamics has been found in academic cases before, with heating of individual building surfaces (Kim and Baik, 2001; Huizhi et al., 2003). Although the changing surface temperature leads to relatively small air temperature differences, the possible change in air flow inside the street canyon can have large consequences on, for instance, pollutant dispersion, as was shown by Baik et al. (2007). Exhaust gases of cars can be trapped in the bottom part of the canyon, or more easily dispersed throughout the canyon, dependent on the flow dynamics.

It must be noted that only the outdoor situation is considered in this study, and that the indoor environment can reveal opposite effects to the outdoor environment. Although Cheng et al. (2005) found a reduction in indoor air temperature when using a high-albedo, Yaghoobian and Kleissl (2012) found the opposite. The reflected radiation is penetrating through the windows, and therefore can increase the indoor temperature. The effect is however very much dependent on the street geometry, albedo and amount of glazing. This indicates that using one adaptation strategy on all locations might give different results, dependent on the local geometry.

The cases considered in this study are highly idealized and only consider a 2D geometry with constant free stream air temperature and wind speed during the summer time. Therefore, the model used can be considered of intermediate complexity. The goal is to include the full 3D arbitrary environment, for which currently steps are undertaken (Tomas et al., 2015; Kenjeres et al., 2015). In addition to the 3D environment, these studies use more advanced turbulence modelling (Large Eddy Simulations in Tomas et al., 2015 and a hybrid RANS-LES model in Kenjeres et al., 2015). Other seasons can also be investigated. For this reason, URBSIM can be coupled (for instance) to a large scale weather model. However, this is currently outside the scope of the current study. In addition to the highly idealized conditions considered in this study, only the building height is changed to obtain different H/W ratios. Using a constant H/W ratio indicates that air flow fields are similar independent of building height or street width. However, this similarity does not hold for the situation at pedestrian level ($z = 2$ m), which is impacted by the actual building height. Qualitative results will not change dramatically, due to the already large building heights used here.

6. Conclusions

This study systematically investigated the effect of different albedo adaptation strategies on surface temperature, air temperature, mean radiant temperature and the UTCI for an idealized 2D street canyon. Using high-albedo materials for all canyon surfaces decreases air temperature but increases the mean radiant temperature more strongly, leading to an increase in the UTCI (indicating more heat stress). This contrasting behaviour of air temperature and mean radiant temperature is observed for all cases. When the UTCI is considered, a higher albedo increases heat stress, which is consistent with the findings from Erell et al. (2014).

The lowest heat stress (within the simplified test cases considered) was found to occur for the case with a vertical gradient of the albedo for $H/W = 1.0$. The gradient used a high albedo at the bottom part of the vertical wall and low albedo near roof level. Air temperature increases slightly compared to a uniform albedo of $\alpha = 0.4$, but reduces the UTCI the most (−2.7 °C). For $H/W = 0.5$, a uniform low albedo of $\alpha = 0.2$ resulted in the largest decrease in heat stress (−1.9 °C) for which the increase in air temperature is compensated by a large decrease in mean radiant temperature.

The present study indicates that there are adverse effects of using high-albedo materials, where air temperature and mean radiant temperature often show opposite responses. It is therefore concluded that simply using high-albedo materials wherever possible might not lead to the desired result of a reduction in the thermal heat stress.

Acknowledgement

We would like to thank Victor Vertregt and Franka Veltman for their help in developing the Monte-Carlo radiation model and the implementation of the mean radiant temperature. This study is funded by the Dutch Climate Proof Cities consortium, which is part of the Knowledge for Climate program (http://knowledgeforclimate.climateresearchnetherlands.nl/climateproofcities).

References

Aida, M., Gotoh, K., 1982. Urban albedo as a function of the urban structure — a two-dimensional numerical simulation. Bound.-Layer Meteorol. 23, 415–424.
Akbari, H., Pomerantz, M., Taha, H., 2001. Cool surfaces and shade trees to reduce energy use and improve air quality in urban areas. Sol. Energy 70, 295–310 (Urban Environment).
Baccini, M., Biggeri, A., Accetta, G., Kostasky, T., Katsouyanni, K., Analitis, A., Anderson, H.R., Bisanti, L., D'Ippoliti, D., Danova, J., Forsberg, B., Medina, S., Paldy, A., Rabczenko, D., Schindler, C., Michelozzi, P., 2008. Heat effects on mortality in 15 European cities. Epidemiology 19, 711–719.
Baik, J.J., Kang, Y.S., Kim, J.J., 2007. Modeling reactive pollutant dispersion in an urban street canyon. Atmos. Environ. 41, 934–949.
Biltoft, C., 2002. Customer report for Mock Urban Test Setting test. Technical Report. Meteorology and Obscurants division. West Desert Test Center, US. Army Dugway Proving Ground.
Bretz, S., Akbari, H., Rosenfeld, A., 1998. Practical issues for using solar-reflective materials to mitigate urban heat islands. Atmos. Environ. 32, 95–101 (Conference on the Benefits of the Urban Forest).
Bröde, P., Fiala, D., Bazejczyk, K., Holmer, I., Jendritzky, G., Kampmann, B., Tinz, B., Havenith, G., 2012. Deriving the operational procedure for the Universal Thermal Climate Index (UTCI). Int. J. Biometeorol. 56, 481–494.
Broede, P., 2005. Universal Temperature Climate Index Documentation. www.utci.org/utci_doku.php.
Brown, G., Delay, M., 2001. Sun, Wind and Light: Architectural Design Strategies. John Wiley and Sons, New York.
Cheng, V., Ng, E., Givoni, B., 2005. Effect of envelope colour and thermal mass on indoor temperatures in hot humid climate. Sol. Energy 78, 528–534.
Durbin, P.A., 1996. On the k–ε stagnation point anomaly. Int. J. Heat Fluid Flow 17, 89–90.
Erell, E., Williamson, T., 2006. Simulating air temperature in an urban street canyon in all weather conditions using measured data at a reference meteorological station. Int. J. Climatol. 26, 1671–1694.
Erell, E., Pearlmutter, D., Boneh, D., Kutiel, P.B., 2014. Effect of high-albedo materials on pedestrian heat stress in urban street canyons. ICUC8: The 8th International Conference on Urban Climate and the 10th Symposium on the Urban Environment. Urban Climate 10, part 2, pp. 367–386.
Fiala, D., Havenith, G., Bröde, P., Kampmann, B., Jendritzky, G., 2012. UTCI-Fiala multi-node model of human heat transfer and temperature regulation. Int. J. Biometeorol. 56, 429–441.
Hilderman, T., Chong, R., 2004. A laboratory study of momentum and passive scalar transport and diffusion within and above a model urban canopy — final report. Technical Report. Coanda Research and Development Corporation, Burnaby.
Huizhi, L., Bin, L., Fengrong, Z., Boyin, Z., Jianguo, S., 2003. A laboratory model for the flow in urban street canyons induced by bottom heating. Adv. Atmos. Sci. 20, 554–564.
Jendritzky, G., de Dear, R., Havenith, G., 2012. UTCI — why another thermal index? Int. J. Biometeorol. 56, 421–428.
Kenjeres, S., Hanjalic, K., 1999. Transient analysis of Rayleigh–Benard convection with a RANS model. Int. J. Heat Fluid Flow 20, 329–340.
Kenjeres, S., Hanjalic, K., 2006. LES, T-RANS and hybrid simulations of thermal convection at high Ra numbers. Int. J. Heat Fluid Flow 27, 800–810.
Kenjeres, S., Hanjalic, K., 2009. Tackling complex turbulent flows with transient RANS. Fluid Dyn. Res. 41, 1–32.
Kenjeres, S., ter Kuile, B., 2013. Modelling and simulations of turbulent flows in urban areas with vegetation. J. Wind Eng. Ind. Aerodyn. 123 (Part A), 43–55.
Kenjeres, S., de Wildt, S., Busking, T., 2015. Capturing transient effects in turbulent flows over complex urban areas with passive pollutants. Int. J. Heat Fluid Flow 51, 120–137.
Kim, J.J., Baik, J.J., 2001. Urban street-canyon flows with bottom heating. Atmos. Environ. 35, 3395–3404.
Lindberg, F., Holmer, B., Thorsson, S., 2008. SOLWEIG 1.0 — modelling spatial variations of 3D radiant fluxes and mean radiant temperature in complex urban settings. Int. J. Biometeorol. 52, 697–713.
Madronich, S., 1987. Photodissociation in the atmosphere: 1. Actinic flux and the effects of ground reflections and clouds. J. Geophys. Res.-Atmos. 92, 9740–9752.
New York High Performance Infrastructure Guidelines, 2005. http://www.nyc.gov/html/ddc/downloads/pdf/hpig.pdf.
Pearlmutter, D., Berliner, P., Shaviv, E., 2007. Integrated modeling of pedestrian energy exchange and thermal comfort in urban street canyons. Build. Environ. 42, 2396–2409.
Philadelphia High Performance Building Renovation Guidelines, 2004. http://www.phila.gov/pdfs/PhiladelphiaGreenGuidelines.pdf.
Santamouris, M., Gaitani, N., Spanou, A., Saliari, M., Giannopoulou, K., Vasilakopoulou, K., Kardomateas, T., 2012. Using cool paving materials to improve microclimate of urban areas — design realization and results of the Flisvos project. Build. Environ. 53, 128–136.
Schrijvers, P.J.C., Jonker, H.J.J., Kenjeres, S., de Roode, S.R., 2015. Breakdown of the night time urban heat island energy budget. Build. Environ. 83, 50–64 (Special Issue: Climate adaptation in cities).

Silva, H.R., Bhardwaj, R., Phelan, P.E., Golden, J.S., Grossman-Clarke, S., 2009. Development of a zero-dimensional mesoscale thermal model for urban climate. J. Appl. Meteorol. Climatol. 48, 567–668.
Simpson, J., McPherson, E., 1997. The effects of roof albedo modification on cooling loads of scale model residences in Tucson, Arizona. Energy Build. 25, 127–137.
Synnefa, A., Dandou, A., Santamouris, M., Tombrou, M., Soulakellis, N., 2008. On the use of cool materials as a heat island mitigation strategy. J. Appl. Meteorol. Climatol. 47, 2846–2856.
Taha, H., Akbari, H., Rosenfeld, A., Huang, J., 1988. Residential cooling loads and the urban heat island: the effects of albedo. Build. Environ. 23, 271–283.
Taha, H., Konopacki, S., Gabersek, S., 1999. Impacts of large-scale surface modifications on meteorological conditions and energy use: a 10-region modeling study. Theor. Appl. Climatol. 62, 175–185.
Theeuwes, N.E., Steeneveld, G.J., Ronda, R.J., Heusinkveld, B.G., van Hove, L.W.A., Holtslag, A.A.M., 2014. Seasonal dependence of the urban heat island on the street canyon aspect ratio. Q. J. R. Meteorol. Soc. 140, 2197–2210.
Thorsson, S., Lindberg, F., Eliasson, I., Holmer, B., 2007. Different methods for estimating the mean radiant temperature in an outdoor urban setting. Int. J. Climatol. 27, 1983–1993.
Tomas, J., Pourquie, M., Jonker, H., 2015. The influence of an obstacle on flow and pollutant dispersion in neutral and stable boundary layers. Atmos. Environ. 113, 236–246.
Tominaga, Y., Yoshie, R., Mochida, A., Kataoka, H., Haricot, K., Nozu, T., 2005. Cross comparison of CFD prediction for wind environment at pedestrian level around buildings (part 2). Proceedings of the Sixth Asia-Pacific Conference on Wind Engineering (APCWE-VI), pp. 2661–2670.
Uehara, K., Murakami, S., Oikawa, S., Wakamatsu, S., 2000. Wind tunnel experiments on how thermal stratification affects flow in and above urban street canyons. Atmos. Environ. 34, 1553–1562.
Vandentorren, S., Suzan, F., Medina, S., Pascal, M., Maulpoix, A., Cohen, J.C., Ledrans, M., 2001. Mortality in 13 French cities during the August 2003 heat wave. Am. J. Public Health 94, 1518–1520.
Whitman, S., Good, G., Donoghue, E., Benbow, N., Shou, W., Mou, S., 1997. Mortality in Chicago attributed to the July 1995 heat wave. Am. J. Public Health 87, 1515–1518.
Yaghoobian, N., Kleissl, J., 2012. Effect of reflective pavements on building energy use. Urban Clim. 2, 25–42.